Sub-diffraction-limited microscopy via Rabi gradient excitation

Xiaodong Zeng,[1,2] Zeyang Liao,[1] M. Al-Amri,[1,2] and M. Suhail Zubairy[1]
[1]*Institute for Quantum Science and Engineering (IQSE) and Department of Physics and Astronomy, Texas A&M University, College Station, Texas 77843-4242, USA*
[2]*The National Center for Applied Physics, KACST, P.O. Box 6068, Riyadh 11442, Saudi Arabia*
(Received 13 March 2015; published 11 June 2015)

We propose a scheme for microscopy with resolution far beyond the diffraction limit by using coherent Rabi oscillations. When the sample is illuminated by a gradient laser field, Rabi oscillations will be induced which can lead to a sinusoidal excitation in the sample. This is similar to the structured illumination microscopy (SIM) which can recover high-spatial-frequency components in the far field. However, different from linear SIM, the sinusoidal pattern here can have a spatial frequency much higher than that of the linear standing wave. Due to this property, we can achieve extremely high resolution, as in the nonlinear saturated SIM, but keep the reconstruction algorithm as simple as the linear one.

DOI: 10.1103/PhysRevA.91.063811 PACS number(s): 42.30.Va, 42.50.Ct, 42.30.Kq

I. INTRODUCTION

Fluorescence light microscopy is widely used as an imaging system because of its inherent parallelism and the fact that its non-ionizing illumination avoids sample damage [1]. However, the resolution of an optical microscope is limited to be about half the wavelength of the fluorescence light which is well known the Abbe diffraction limit [2,3]. Although electron microscopy can give super-resolution, it may ionize and damage the sample [4]. Scanning tunneling microscopy can also achieve extremely high resolution, but it is surface bound and has limited applications [5,6]. In the past two decades, a number of methods have been proposed to overcome the diffraction limit in fluorescence light microscopy [7–30]. One way to achieve super-resolution is by reducing the effective point spread function (PSF) such as photoactivated localization microscopy (PALM) [9], stochastic optical reconstruction microscopy (STORM) [10], and stimulated-emission depletion (STED) microscopy [11–15]. However, STED microscopy requires point-by-point scanning which leads to a very low speed. Although PALM and STORM can image multiple molecules within a sample in parallel, only one molecule within one diffraction-limited spot is excited at a time. In addition, to precisely localize a molecule, multiple detections need to be performed. Therefore, PALM and STORM also require an extended time to acquire a super-resolution image.

Different from the super-resolution methods where the effective point spread function is reduced, there is another type of method which can achieve super-resolution by recovering the high-spatial-frequency components in the far field, such as the metamaterial-based lens [16–18] and structured illumination microscopy [19–25]. The evanescent wave with high spatial frequency can propagate in the metamaterial with negative reflective index. High-spatial-frequency information can be acquired when using a metamaterial-based lens. However, the lens in this method needs to be placed in the near-field regime of the sample and it is surface bound which has limited applications. In structured illumination microscopy (SIM), by illuminating the sample with a sinusoidal standing wave, high-spatial-frequency information may be transferred to the observable regime based on the Moiré effect. A super-resolution image can be obtained by numerical reconstruction. In linear SIM, the resolution can be enhanced by a factor of 2 [19]. In nonlinear saturated SIM by the saturated absorption, higher resolution may be obtained [24,25]. However, the nonlinear saturated illumination requires very high power and the reconstruction mathematics is very complicated because many higher-order terms are involved.

Inspired by our subwavelength optical lithography scheme via coherent Rabi oscillations [31–33], here we propose a super-resolution microscopy which is termed coherent Rabi gradient excitation microscopy (CORAGEM). Different from SIM, the structured illumination is achieved by gradient Rabi oscillations. The atoms in the sample can be periodically prepared in the excited state with spatial wavelength much smaller than the wavelength of the driving light. The atoms in the excited state can then emit fluorescence and be detected in the far field. This process is equivalent to the structured illumination by a light with very high frequency where we can transfer the high-spatial-frequency information into the observable region. However, in our proposal we do not need high-frequency light. Although the nonlinear saturated SIM (SSIM) can also achieve very high resolution without high-frequency light, the reconstruction mathematics here is much simpler than that of SSIM because in our proposal only three wave vectors are involved in one detection.

The paper is organized as follows. In Sec. II, we introduce our model and theory. In Sec. III, numerical simulations of the reconstructed images are presented. Section IV is the conclusion.

II. MODEL AND THEORY

The proposed setup is shown in Fig. 1(a). Two Gaussian pulses with full width at half maximum (FWHM) of the intensity $t_{\mathrm{FWHM}} = 2\sqrt{\ln 2}\sigma$ are incident on the imaging sample from opposite directions, making an angle θ with the horizontal. A time-dependent standing wave can be formed as

$$E(x,t) = 2E_0 \exp\left(-\frac{t^2}{2\sigma^2}\right)\exp(-i\omega t)\cos(k_0 x\cos\theta+\varphi), \tag{1}$$

where E_0 is the electric field amplitude, φ is the phase difference between the two pulses, ω is the laser frequency which is resonant with the transition frequency between

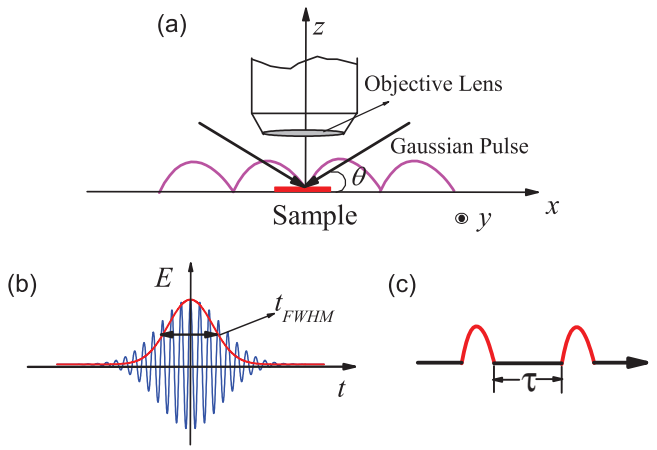

FIG. 1. (Color online) (a) Two Gaussian pulses irradiate the imaging sample. The sample is in the x-y plane. (b) The Gaussian pulse. The red line is the intensity profile. (c) The pulses irradiate the sample periodically with pulse separation τ.

the excited state $|e\rangle$ and the ground state $|g\rangle$ of the atoms in the sample, and $k_0 = \omega/c$ is the vacuum wave number. The dynamics of the atomic system satisfies the following equations [34]:

$$\begin{aligned}\dot{\rho_{ee}} &= -\gamma_e\rho_{ee} - 2\mathrm{Im}[\Omega(x,t)\rho_{ge}],\\ \dot{\rho_{gg}} &= \gamma_e\rho_{ee} + 2\mathrm{Im}[\Omega(x,t)\rho_{ge}],\\ \dot{\rho_{eg}} &= -\left(\frac{\gamma_e}{2}+\gamma_{eg}\right)\rho_{eg} - i\Omega(x,t)(\rho_{ee}-\rho_{gg}).\end{aligned} \tag{2}$$

Here, γ_e is the decay rate while γ_{eg} is the dephasing rate. $\Omega(x,t)$ is the Rabi frequency depending on the time and position, i.e., $\Omega(x,t) = 2|\wp_{eg}|E_0\exp(-t^2/2\sigma^2)\cos(kx\cos\theta + \varphi)/\hbar$, where $|\wp_{eg}|$ is the transition dipole moment between levels $|e\rangle$ and $|g\rangle$.

Ignoring the dissipation process, after the pulse, the spatial distribution of the upper-level population is given by [31]

$$P_e(x) = \frac{1-\cos[\Omega_0 t_0\cos(k_0 x\cos\theta+\varphi)]}{2}, \tag{3}$$

where $\Omega_0 = 2E_0|\wp_{eg}|/\hbar$ and $t_0 = \sqrt{\pi/2\mathrm{In}2}\,t_{\mathrm{FWHM}}$. Assuming that θ is large such that $k_0 x\cos\theta \ll 1$ and $\varphi \to \pi/2$, we have

$$P_e(x) \approx \frac{1-\cos(2k_{\mathrm{eff}}x+\varphi_{\mathrm{eff}})}{2}, \tag{4}$$

where

$$k_{\mathrm{eff}} = \Omega_0 t_0 k_0\cos\theta/2, \varphi_{\mathrm{eff}} = \Omega_0 t_0(\varphi-\pi/2). \tag{5}$$

The excitation probability has a sinusoidal pattern with effective spatial frequency depending on the Rabi frequency and the pulse duration; k_{eff} can be much larger than k_0 if $\Omega_0 t_0\cos\theta \gg 1$. This is critical for the super-resolution technique here. We can also control the Rabi frequency, pulse duration, and initial phase difference φ to tune the effective wave number k_{eff} and the phase shift φ_{eff}.

The driving pulse needs to be shorter than the decay and dephasing time because the coherent Rabi oscillations can be damped when the system decays. For full dynamics, we need to numerically solve Eqs. (2)–(4). A numerical example is shown in Fig. 2 where we set $\cos\theta = 0.1$, $\Omega_0 = 2E_0|\wp_{eg}|/\hbar = 10^{13}$ s^{-1}, $t_{\mathrm{FWHM}} = 6\sqrt{\mathrm{In}2}$ ps, $\varphi = 0$, and $\gamma_e = \gamma_{eg} = 5\times 10^9$ s^{-1}. It is shown that near the node of the standing wave the electric field is nearly linear versus the position and the excited population shows an approximately sinusoidal pattern with period much smaller than the usual diffraction limit, i.e., $\lambda_0/2$.

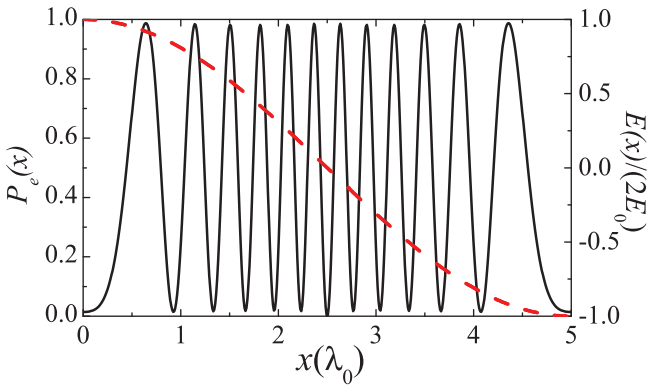

FIG. 2. (Color online) The black solid curve denotes the population of the excited state versus the position after the Gaussian pulses. The red dashed line is the electric field at $t = 0$. $\lambda_0 = 2\pi c/\omega$ is the vacuum wavelength.

The derivative $\sin(k_0 x\cos\theta)$ of the electric field determines the density of the peaks. In Fig. 2, we can see that near the node, $\sin(k_0 x\cos\theta)$ reaches the maximum, which leads to the smallest period of the population. This is the reason that we set the sample in this region.

In Ref. [30], the authors used a similar method to localize an atom based on the fact that an atom in a different position undergoes different Rabi cycles in a Gaussian-type illumination spot. In the following, we show that we can exploit this exciting property to propose a scheme for sub-diffraction-limited microscopy. Of course, due to the spontaneous decay and dephasing, the sinusoidal pattern is not perfect [31], which can affect the precision of the scheme. However, if the pulse duration is much smaller than the decay time, the dissipation effects can be neglected. In the following calculation, we do not consider these effects and we analyze them in the last part of Sec. III.

After the excitation, the atoms in the excited state emit fluorescence which is detected in the far field. According to the Fourier optics, the image spectrum for two-dimensional fluorescence microscopy can be described as [19–25]

$$i(k_x,k_y) = \phi(k_x,k_y)t(k_x,k_y), \tag{6}$$

where $i(k_x,k_y)$ is the Fourier expansion of the observed image function $I(x,y)$, $\phi(k_x,k_y)$ is the unknown spatial frequency spectrum of the emitting atoms, and $t(k_x,k_y)$ is the optical transfer function (OTF), which is the Fourier transformation of the point spread function and dependent on the lens of the microscopy; $t(k_x,k_y)$ can be predetermined by some detections and calculations. Because only the field with $\rho \leqslant A_N k_0$ contributes to the image in a far-field fluorescence microscopy, where k_0 is the vacuum wave number, A_N is the numerical aperture of the objective lens and ρ is the wave vector parallel to the image plane. Only the corresponding spatial frequency components within the passband $\sqrt{k_x^2+k_y^2} = k_{||} \leqslant 2A_N k_0 = \kappa$

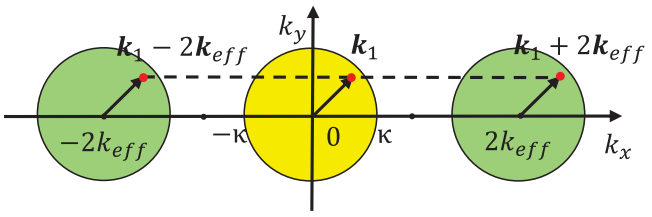

FIG. 3. (Color online) Diagram of the spatial frequency. The yellow circle on the origin is the range contributing to the conventional microscopy. The green circles with center points at $\pm 2k_{\text{eff}}$ are the effects of Gaussian pulses.

can be observed due to the OTF being nonzero only in this region. From $i(k_x,k_y)$ and $t(k_x,k_y)$, we can then determine $\phi(k_x,k_y)$.

The spatial frequency spectrum $\phi(k_x,k_y)$ is the Fourier transformation of the emission pattern $\Phi(x,y)$. Similar to the "Moiré effect" in the traditional linear SIM, the emission pattern is given by [15]

$$\Phi(x,y) = P_e(x,y)F(x,y), \tag{7}$$

where $F(x,y)$ is the unknown spatial distribution of the atoms in the sample and $P_e(x,y)$ is the atomic excitation distribution given by Eq. (4). Supposing the excitation has a sinusoidal pattern along the x direction, by performing the Fourier transformation and neglecting the common constant factor we obtain

$$\begin{aligned}\phi(k_x,k_y) = {} & 2f(k_x,k_y) + f(k_x - 2k_{\text{eff}},k_y)e^{i\varphi_{\text{eff}}} \\ & + f(k_x + 2k_{\text{eff}},k_y)e^{-i\varphi_{\text{eff}}}.\end{aligned} \tag{8}$$

Here k_{eff} and φ_{eff} are given by Eq. (5) and $f(k_x,k_y)$ is the Fourier transformation of $F(x,y)$. Since k_{eff} can be much larger than k_0, high-spatial-frequency information can be coupled into the observable region (Fig. 3). Therefore, $\phi(k_x,k_y)$ calculated from Eq. (6) encodes the information of the three spatial frequency components ($k_x - 2k_{\text{eff}}$, k_x, and $k_x + 2k_{\text{eff}}$). Each fluorescence image is formed by the spatial frequency components in three circles with centers at $-2k_{\text{eff}}$, 0, and $2k_{\text{eff}}$, respectively. The three frequency components in the three circles can be completely determined from three fluorescence images by changing the phase shift φ_{eff}. To reconstruct all the frequencies between k_0 and $2k_{\text{eff}}$ along the x axis, we can tune either the pulse intensity or the pulse duration to control the Rabi frequency and then k_{eff}. Rotating the x axis around the origin, we can obtain all the spatial frequencies in the two-dimensional space with a radius $2k_{\text{eff}}^{\max} + \kappa$. The inverse Fourier transformation of $f(k_x,k_y)$ is the super-resolution image. The mathematics here is as simple as that in linear SIM. However, the resolution here can be enhanced by a factor much larger than 2 in conventional linear SIM.

III. NUMERICAL SIMULATION

In Fig. 4, we present the image simulation with conventional microscopy and two image reconstruction simulations based on our super-resolution microscopy method. We assume that the driving laser has a wavelength of 500 nm, $A_N = 1$, and $|\wp_{eg}| = 10$ D [35]. In Fig. 4(b), we present the sample image

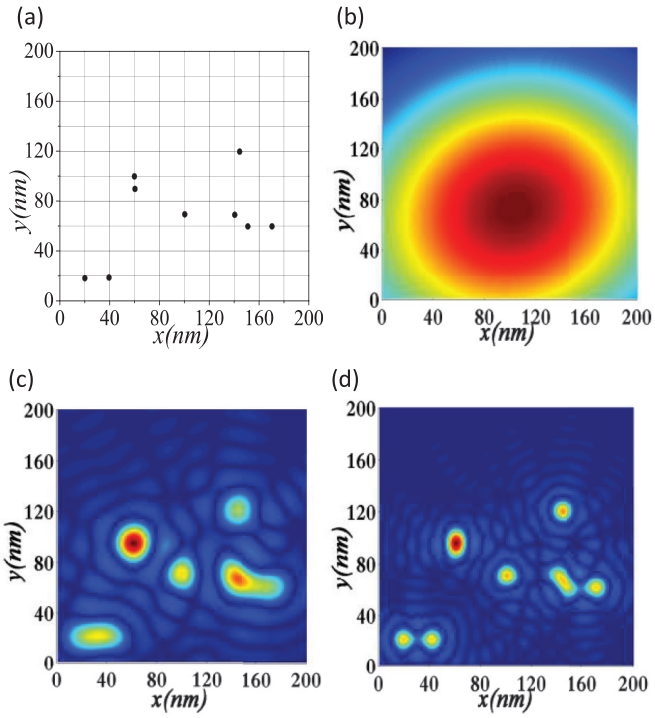

FIG. 4. (Color online) (a) The distribution of the sample atom. (b) The sample image with a conventional microscopy. (c) The image simulation with pulse intensity 59.8 MW cm^{-2} and $t_{\text{FWHM}} = 150$ ps. (d) The image simulation with pulse intensity 89.7 MW cm^{-2} and $t_{\text{FWHM}} = 200$ ps. The other parameter is $\cos\theta = 0.05$.

with conventional microscopy. Here, we assume the induced polarization of the sample atom is perpendicular to the sample plane, which can save calculation time compared with the assumption that the induced atomic polarization is parallel to the sample plane. It is shown that no spatial information of the sample atom can be obtained as the separations between the atoms are much smaller than the diffraction limit, i.e., 250 nm. In the reconstruction simulations of our method, the polarizations of the pulses are perpendicular to the incident plane and the direction of the induced transition dipole moments of the sample atoms are also perpendicular to the incident plane. In Fig. 4(c), we present the numerical result when the pulse intensity is 59.8 MW cm^{-2} and $t_{\text{FWHM}} =$ 150 ps. We can calculate $k_{\text{eff}} = 6k_0$, which can result in a 6 times resolution enhancement. Indeed, we can resolve some sub-diffraction features which is forbidden by the traditional microscopy. However, there are some atoms which are too close to be resolved. When we increase the pulse intensity to be 89.7 MW cm^{-2} and $t_{\text{FWHM}} = 200$ ps, the numerical result is shown in Fig. 4(d). We can see that some unresolved features in Fig. 4(c) are now resolved because here $k_{\text{eff}} = 12k_0$, which can result in a 12-fold resolution enhancement. The resolution in Fig. 4(c) is about 40 nm, while the resolution in Fig. 4(d) is about 20 nm. The field intensity in our simulation is five orders lower than that used in the two-photon microscopy [7,8] or two orders weaker than the STED microscopy [11,14] and is at the same level as conventional SIM [19,24].

Different from other super-resolution microscopies like STED and SIM, our method here is a coherent technique

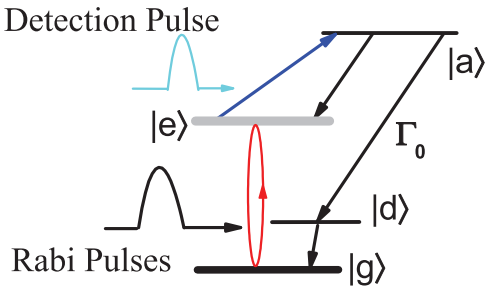

FIG. 5. (Color online) The sample atom structure. The atom can decay from level $|a\rangle$ to $|e\rangle$ and $|d\rangle$ spontaneously.

where the Rabi oscillations need to be performed within the population decay time of the system. In the simulations of Fig. 4, the decay rate is about $\omega^3|\wp|^2/(3\varepsilon_0\hbar c^3) \approx 1.8 \times 10^6$ s^{-1} [34], where ε_0 is vacuum permittivity and c is the vacuum optical velocity. Additionally, the dephasing rate is about one order larger than the decay rate. If we did not consider the influence of the decay and dephasing of the sample, there would be error due to the atomic population after the pulses not having an exactly sinusoidal distribution. In order to decrease this effect, small decay and dephasing rate as well as short pulses can be chosen. For the parameters used in Fig. 2, we have $t_{\mathrm{FWHM}} \ll \frac{1}{\gamma_e,\gamma_{eg}}$, and we can safely neglect the dissipation of the system. In a real experiment, if the pulse duration is too short, we must choose a high-intensity pulse to get an effectively large wave number, which may damage the sample. If the decay and dephasing rates are small, the period of the pulses τ must be large enough to guarantee the atom to be back to the ground state, which will slow the imaging process. Hence, we should balance the imaging velocity and the pulse intensity.

The decay and dephasing rate γ_e and γ_{eg} can be chosen to be the same as those in Fig. 2, and τ to be 1×10^{-6} s. We assume a 0.1 photon collection efficiency. In 1 s, we can collect, on average, 1×10^5 photons from one atom. For the parameters in Fig. 4(c), we approximately need 200 images total, which also needs a relatively long time as in conventional SIM [22–25], i.e., tens of seconds.

In a real experiment, the incident pulse source and the objective can be placed at opposite sides of the sample [21], so we can control the incident angle of the pulses conveniently. To eliminate the interruption of the illumination field, we can employ additional energy levels of the atom as shown in Fig. 5 [23]. After the Rabi oscillations, we use an additional detection pulse which is normal incident to the sample plane to drive the atom from $|e\rangle$ to $|a\rangle$. The detection pulse only covers the region where the illumination field is linear. In the imaging process, we can use a dichroic mirror and a bandpass filter to detect the photons emitted from $|a\rangle$ to $|d\rangle$ with frequency ω_{ad} but not from the illumination field [21,24]. The probability that an atom in the detection pulse domain goes from level $|e\rangle$ to $|d\rangle$ is denoted as $G(x,y)$, which is dependent on the detection pulse intensity distribution and can be predetermined. The final reconstructed image is equal to the case of replacing $F(x,y)$ in Eq. (7) with $F(x,y)G(x,y)$ from which we can determine the spatial distribution of the sample $F(x,y)$. By shifting the position of the detection pulse, we can reconstruct the image in a different region. By repeating these procedures, we can image an arbitrary large area. Although it takes longer time to image a large area, our method should still have a speed advantage over the methods based on point-by-point scanning because our method here is based on area-by-area scanning.

IV. CONCLUSION

In conclusion, we propose a scheme for super-resolution microscopy via quantum coherent Rabi oscillations. By applying a laser pulse with frequency resonant to two atomic levels of the sample and with electric field strength gradient in the space, we can prepare the atoms in the excited state with a sinusoidal spatial distribution. The period of the sinusoidal pattern can be much smaller than the excitation wavelength if the pulse area is large enough. This is equivalent to a linear response to a standing wave with very large wave number which can subsequently couple the high-spatial-frequency components into the observable region. By performing the reconstruction algorithm, we can obtain a super-resolution image. Our method requires that the system has a relatively long coherence time. However, there are a lot of interesting systems such as biological molecules which has very short coherence time. Our method cannot directly apply to these systems. Despite that, we may suitably dye molecules or nanoparticles which have energy levels with long coherence time to mark the sample. Although the reconstruction algorithm is as simple as linear SIM, our method here can achieve a resolution much higher than that of linear SIM. The nonlinear saturated SIM can also achieve high resolution, but the reconstruction algorithm is much more complicated than our method here. Therefore, the reconstruction errors can be largely reduced in our proposal.

ACKNOWLEDGMENTS

This research is supported by NPRP Grant No. 7-210-1-032 from the Qatar National Research Fund (QNRF) and a grant from King Abdulaziz City for Science and Technology (KACST).

[1] *Nanoscopy and Multidimensional Optical Fluorescence Microscopy*, edited by A. Diaspro (CRC Press, Boca Raton, FL, 2010).
[2] E. Abbe, Arch. Mikr. Anat. **9**, 413 (1873).
[3] L. Rayleigh, Philos. Mag. **8**, 261 (1879).
[4] R. Erni, M. D. Rossell, C. Kisielowski, and U. Dahmen, Phys. Rev. Lett. **102**, 096101 (2009).
[5] G. Binnig, C. F. Quate, and C. Gerber, Phys. Rev. Lett. **56**, 930 (1986).
[6] C. Hettich, C. Schmitt, J. Zitzmann, S. Kühn, I. Gerhardt, and V. Sandoghdar, Science **298**, 385 (2002).
[7] W. Denk, J. H. Strickler, and W. W. Webb, Science **248**, 73 (1990).
[8] J. H. Strickler and W. W. Webb, Proc. SPIE **1398**, 107 (1991).

[9] E. Betzig, G. H. Patterson, R. Sougrat, O. W. Lindwasser, S. Olenych, J. S. Bonifacino, M. W. Davidson, J. L. Schwartz, and H. F. Hess, Science **313**, 1642 (2006).
[10] M. J. Rust, M. Bates, and X. Zhuang, Nat. Methods **3**, 793 (2006).
[11] S. W. Hell and J. Wichmann, Opt. Lett. **19**, 780 (1994).
[12] S. W. Hell and M. Kroug, Appl. Phys. B **60**, 495 (1995).
[13] V. Westphal and S. W. Hell, Phys. Rev. Lett. **94**, 143903 (2005).
[14] D. Wildanger, J. R. Maze, and S. W. Hell, Phys. Rev. Lett. **107**, 017601 (2011).
[15] T. A. Klar, S. Jakobs, N. Dyba, A. Egner, and S. W. Hell, Proc. Natl. Acad. Sci. USA **97**, 8206 (2000).
[16] Z. Liu, H. Lee, Y. Xiong, C. Sun, and X. Zhang, Science **315**, 1686 (2007).
[17] X. Zhang and Z. Liu, Nat. Mater. **7**, 435 (2008).
[18] D. Lu and Z. W. Liu, Nat. Commun. **3**, 1205 (2012).
[19] M. G. L. Gustafsson, J. Microsc. (Oxford, UK) **198**, 82 (2000).
[20] R. Heintzmann, T. M. Jovin, and C. Cremer, J. Opt. Soc. Am. A **19**, 1599 (2002).
[21] J. T. Frohn, H. F. Knapp, and A. Stemmer, Proc. Natl. Acad. Sci. USA **97**, 7232 (2000).
[22] F. Wei and Z. Liu, Nano Lett. **10**, 2531 (2010).
[23] X. D. Zeng, M. Al-Amri, and M. S. Zubairy, Phys. Rev. B **90**, 235418 (2014).
[24] M. G. L. Gustafsson, Proc. Natl. Acad. Sci. USA **102**, 13081 (2005).
[25] L. Schermelleh, P. M. Carlton, S. Haase, L. Shao, L. Winoto, P. Kner, B. Burke, M. C. Cardoso, D. A. Agard, M. G. L. Gustafsson, H. Leonhardt, and J. W. Sedat, Science **320**, 1332 (2008).
[26] D. D. Yavuz and Z. J. Simmons, Phys. Rev. A **86**, 013817 (2012).
[27] S. Qamar, J. Evers, and M. S. Zubairy, Phys. Rev. A **79**, 043814 (2009).
[28] H. B. Li, V. A. Sautenkov, M. M. Kash, A. V. Sokolov, G. R. Welch, Y. V. Rostovtsev, M. S. Zubairy, and M. O. Scully, Phys. Rev. A **78**, 013803 (2008).
[29] Z. Liao, M. Al-Amri, and M. S. Zubairy, Phys. Rev. A **85**, 023810 (2012).
[30] I. Gerhardt, G. Wrigge, J. Hwang, G. Zumofen, and V. Sandoghdar, Phys. Rev. A **82**, 063823 (2010).
[31] Z. Liao, M. Al-Amri, and M. Suhail Zubairy, Phys. Rev. Lett. **105**, 183601 (2010).
[32] Z. Liao, M. Al-Amri, T. Becker, W. P. Schleich, M. O. Scully, and M. S. Zubairy, Phys. Rev. A **87**, 023405 (2013).
[33] Z. Liao, M. Al-Amri, and M. S. Zubairy, Phys. Rev. A **88**, 053809 (2013).
[34] M. O. Scully and M. S. Zubairy, *Quantum Optics* (Cambridge University Press, Cambridge, UK, 1997).
[35] P. C. Becker, R. L. Fork, C. H. Brito Cruz, J. P. Gordon, and C. V. Shank, Phys. Rev. Lett. **60**, 2462 (1988).